

# Formation of voids in the Universe within the Lemaître–Tolman model

Krzysztof Bolejko,<sup>1</sup>\*† Andrzej Krasiński<sup>2</sup>† and Charles Hellaby<sup>3</sup>†

<sup>1</sup>*Department of Physics, Astronomical Observatory, University of Warsaw, Aleje Ujazdowskie 4, 00-478 Warsaw, Poland*

<sup>2</sup>*Nicolaus Copernicus Astronomical Center, Polish Academy of Science, ul. Bartycka 18, 00-716 Warsaw, Poland*

<sup>3</sup>*Department of Mathematics and Applied Mathematics, University of Cape Town, Rondebosch 7700, Cape Town, South Africa*

Accepted 2005 June 9. Received 2005 June 8; in original form 2004 November 30

## ABSTRACT

We develop models of void formation starting from a small initial fluctuation at recombination and growing to a realistic present-day density profile in agreement with observations of voids. The model construction is an extension of previously developed algorithms for finding a Lemaître–Tolman metric that evolves between two profiles of either density or velocity specified at two times. Of the four profiles of concern (those of density and velocity at recombination and at the present day), two can be specified and the other two follow from the derived model.

We find that, in order to reproduce the present-day void density profiles, the initial velocity profile is more important than the initial density profile.

Extrapolation of current cosmic microwave background (CMB) observations to the scales relevant to protovoids is very uncertain. Even so, we find that it is very difficult to make both the initial density and velocity fluctuation amplitudes small enough and still obtain a realistic void by today.

**Key words:** cosmic microwave background – cosmological parameters – cosmology: theory – early Universe – large-scale structure of Universe.

## 1 AIM

Voids are vast regions of the Universe with a high negative density contrast, which are fundamental parts of the large-scale structure of the Universe. Although the mean radius of voids is  $10 h^{-1}$  Mpc, they contain only a few galaxies. According to the data from the 2-degree Field Galaxy Redshift Survey (2dFGRS)<sup>1</sup> processed by Hoyle & Vogeley (2004), about 40 per cent of the volume of the Universe is taken up by voids.

The aim of this paper is to describe the non-linear growth of voids out of small initial density and velocity perturbations on a homogeneous background at the moment of last scattering. We intend to remain within the solidly established physics and to do without unobservable entities that are currently in vogue, like cold dark matter. We use the inhomogeneous, spherically symmetric dust (Lemaître–Tolman; L–T) model, an exact solution of Einstein’s equations. This paper also reports on the main factors responsible for the formation of voids, and a simulation of void evolution is presented. As follows from our previous papers (Krasiński & Hellaby 2002, 2004), the final state is sensitive not just to the amplitude, but also to the

exact profile of the initial perturbations. So although velocity perturbations of relative amplitude ( $\Delta V/V$ ) around  $8 \times 10^{-3}$  were needed in our models to reproduce realistic voids, it is still possible that other profiles can be found for which a smaller initial velocity amplitude will suffice.

## 2 A HISTORICAL OVERVIEW

The discovery of large-scale cosmic voids became possible when astronomers started to measure the distribution of galaxies in space. Since William and John Herschel’s researches, i.e. from 19th century, it was known that galaxies cluster (for example in the Virgo or Coma cluster). However, there could be no certainty that these clusters were not just caused by the galaxies being projected on the celestial sphere. This changed with the publication of the Hubble law in 1929. Five years later Tolman (1934) and, immediately after, Sen (1934) studied the stability of the Friedmann models with respect to inhomogeneous perturbations and concluded that they are unstable against a rarefaction caused by a negative perturbation of either the initial density or the initial velocity. Consequently, there should be condensations as well as underdense regions in the Universe.

Nevertheless, it was only at the end of 1970s that voids were discovered. However, the very first sign of their existence had been known 20 yr earlier. In 1960, Mayall had measured the redshift of 50 galaxies in the Coma cluster (Mayall 1960). His survey covered  $33 \text{ deg}^2$  of the celestial sphere. The Coma cluster was also studied by Chincarini & Rood (1975), but it was the large survey of Gregory

\*Present address: Nicolaus Copernicus Astronomical Centre, Bartycka 18, 00-716 Warszawa, Poland.

†E-mail: bolejk@camk.edu.pl (KB); akr@camk.edu.pl (AK); cwh@maths.uct.ac.za (CH)

<sup>1</sup> <http://www.aao.gov.au/2df>

**Table 1.** The void hierarchy (from Lindner et al. 1996).

Type of object	Mean size
Rich clusters (Abell Catalogue)	100 $h^{-1}$ Mpc
Poor clusters (Zwicky Catalogue)	37 $h^{-1}$ Mpc
Bright ( $M \leq -20.3$ ) elliptical galaxies	30 $h^{-1}$ Mpc
Galaxies brighter than $M = -20.3$	23 $h^{-1}$ Mpc
Galaxies brighter than $M = -19.7$	16 $h^{-1}$ Mpc
Galaxies brighter than $M = -18.8$	13 $h^{-1}$ Mpc

& Thompson (1978) that ended with the discovery of a void. Their survey covered 260 deg<sup>2</sup> of the sky and comprised galaxies up to 15th magnitude, which is equivalent to a radial velocity of approximately 8000 km s<sup>-1</sup>.

Also, Jõeveer, Einasto & Tago (1978) observed voids in their redshift survey. At the beginning of 1980s the term ‘void’ was first used to call the regions avoided by galaxies (Rood 1988).

Next, researchers discovered extremely large regions avoided by galaxies called supervoids. The classical example is the void discovered by Kirshner et al. (1981). From the late 1970s, they were observing the galaxies in the Bootes and Corona Borealis constellation and discovered an almost empty region with the size of 50–100  $h^{-1}$  Mpc, (where  $h$  is the Hubble parameter in units of 100 km s<sup>-1</sup> Mpc<sup>-1</sup>). More up-to-date measurements determine this size to be approximately 60  $h^{-1}$  Mpc and prove that this region is not entirely empty. Dey, Strauss & Huchra (1990) observed 21 galaxies within this region and estimated the mean density contrast to be

$$\delta = \frac{\rho_{\text{mat}} - \overline{\rho_{\text{mat}}}}{\overline{\rho_{\text{mat}}}} \in (-0.84, -0.66), \quad (1)$$

where  $\rho_{\text{mat}}$  and  $\overline{\rho_{\text{mat}}}$  are the density and mean density of matter in the Universe.

Other discoveries of voids followed very fast. In 1982, after a five year survey, the Centre for Astrophysics (CfA) galaxy redshift catalogue was finished. Huchra et al. (1983) measured redshifts for over 2400 galaxies with luminosity below magnitude 14.5. The amount of data increased in later surveys. For example, the current Sloan Digital Sky Survey (SDSS)<sup>2</sup> covers one-fourth of the celestial sphere and will measure redshifts for over 10<sup>8</sup> objects.

### 3 SIZES AND SHAPES OF THE VOIDS

The size of a void depends on the luminosity of the galaxies that surround it. The research done by Lindner et al. (1995) has shown that the mean void size, as estimated by bright elliptical galaxies, varies between 13 and 36  $h^{-1}$  Mpc, whereas the size evaluated by the measurement of fainter galaxies drops to 9–25  $h^{-1}$  Mpc. This phenomenon is known as the void hierarchy, whose characteristics are listed in Table 1 (Lindner et al. 1996).

According to the data from the 2dFGRS, the average radii of voids in the North Galactic Pole (NGP) and in the South Galactic Pole (SGP) are  $14.89 \pm 2.67$  and  $15.61 \pm 2.48$   $h^{-1}$  Mpc respectively (Hoyle & Vogeley 2004). The maximal radius of a sphere inscribed into a void is  $12.09 \pm 1.85$   $h^{-1}$  Mpc in NGP and  $12.52 \pm 1.99$   $h^{-1}$  Mpc in SGP. These sizes were estimated using galaxies whose luminosity  $M_{\text{lim}} - 5 \log(h)$  varied from  $-18$  to  $-21$ .

The computer algorithm employed by Hoyle and Vogeley in their void search used a similar rule to that invented by El-Ad & Piran (1997). Firstly, the algorithm decides whether a particular galaxy

should be assigned to the wall (a region of higher density surrounding the void) or to the void itself. Then the voids are filled with spheres.

It is apparent that the shapes of small voids are close to spherical, while the largest voids are more irregular. However, they can still be divided into smaller spherical voids. Sato (1982, 1984) hypothesized that spherical voids collide with each other as they expand, to produce Zeldovich’s ‘pancakes’. The fact that large non-spherical voids can be divided into spherical regions may thus indicate that they are conglomerates of smaller spherical voids that had already collided. Together with another result that for voids the spherical shape is stable (Sato & Maeda 1983), this shows that the L–T solution is the right device to model voids.

### 4 DENSITY CONTRAST

While considering the above data, the following question arises: are these regions really empty? Or are some objects just not bright enough to be detected by galaxy surveys? This issue was investigated by Thuan, Gott & Schneider (1987). They examined the distribution of faint, dwarf and irregular galaxies from the Nilson Uppsala General Catalogue of Galaxies (UGC) and concluded that faint galaxies do not form any separate large-scale structures but occur together with bright galaxies. Similar results were obtained by Peebles (2001), who analysed the data from the Optical Redshift Survey (ORS). The conclusion is that, because there are no bright galaxies in voids, there should be no faint ones, either. Some observational studies of dwarf galaxies in the nearest neighbourhood (Pustil’nik et al. 1995; Kuhn, Hopp & Elsaesser 1997; Popescu, Hopp & Elsaesser 1997; Grogin & Geller 1999) found galaxies in voids. However, these were only single objects, so the deduction of Thuan et al. (1987) and Peebles (2001) was qualitatively right. Today voids are defined as regions of low density, or as regions avoided by certain type of objects, for example bright galaxies. According to these definitions, voids do not have to be empty. Rojas et al. (2004) focused on the photometrical properties of galaxies in the voids from the SDSS data. They defined the voids as regions of density contrast  $\delta \leq -0.6$ . In their study, they measured galaxies up to  $z = 0.089$ . From 155 000 galaxies they extracted a sample of 13 742, in which 1010 were galaxies in voids. Their analysis shows that galaxies in voids are fainter, more blue and more compact than galaxies in the walls.

Of the galaxies from the 2dFGRS, 5 per cent are void galaxies. The average density contrast for voids in this survey is presented in Fig. 1. The mean density contrast in the central region is  $\delta = -0.94 \pm 0.02$  in NGP and  $\delta = -0.93 \pm 0.02$  in SGP.

However, data obtained from observations of galaxies give information about the luminous matter, while dark matter does not have to concentrate in galaxies. Peebles (2001), referring to the existing radio-astronomical observations of 21-cm waves (sensitive to H I clouds; Weinberg et al. 1991; Hoffman, Lu & Salpeter 1992; Szomoru et al. 1996; Zwaan et al. 1997) and to the results of observations of Lyman  $\alpha$  absorption line system (Bergeron & Boisse 1991; Steidel, Dickinson & Persson 1994; Lanzetta et al. 1995), concluded that not only galaxies but also gas clouds avoid voids. This conclusion can only be justified indirectly because there are no direct observations of Lyman  $\alpha$  clouds in voids.

The voids that are discovered in surveys are defined by galaxies with low redshift. For example, the maximal redshift used by Hoyle & Vogeley (2004) to find voids in the 2dFGRS was  $z = 0.138$ . For such a small redshift, the Lyman  $\alpha$  line ( $\lambda = 1216 \text{ \AA}$ ) is in the ultraviolet, which is beyond the reach of observations from the ground. The

<sup>2</sup> www.sdss.org

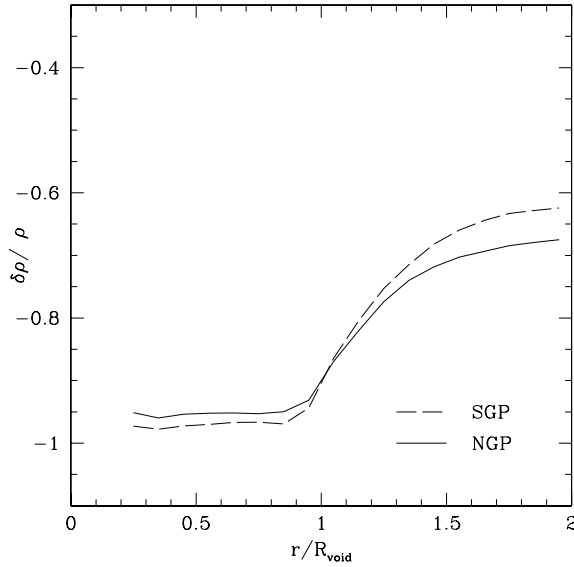


**Figure 1.** The average density contrast for voids in the 2dFGRS, in units of void radius (figure taken from Hoyle & Vogeley 2004).

resolution of the *IUE* (*International Ultraviolet Explorer*) satellite was not sufficient to detect the Lyman  $\alpha$  clouds.

One must ask whether luminous matter is a good tracer of mass, or is there a significant amount of dark matter within voids? Is the density contrast for dark matter the same as for luminous matter, or do galaxies prefer regions of higher density contrast? In the second case, the real density contrast would not be as low as the one in Fig. 1.

Answers to these questions suggested by cold dark matter  $N$ -body simulations are inconclusive. In these simulations, the positions of test particles in a chosen part of space are traced. Progress in this field depends on the computing power. Arbabi-Bidgoli & Muller (2002) used  $256^3$  particles of masses  $10^{11} h^{-1} M_{\odot}$  and  $4 \times 10^{10} h^{-1} M_{\odot}$ . They obtained density contrasts from  $\delta \sim -0.6$  for the voids with the mean diameter  $10\text{--}16 h^{-1}$  Mpc to  $\delta \sim -0.8$  for the voids with mean diameter  $36\text{--}50 h^{-1}$  Mpc. Benson et al. (2003) used  $512^3$  particles of masses  $10^9 h^{-1} M_{\odot}$ . Their simulations implied that the density contrast should be  $\delta \sim -0.8, 0.85$ . Gottlöber et al. (2003) used  $1024^3$  particles of  $4 \times 10^7 h^{-1} M_{\odot}$  and obtained the density contrast of approximately  $\delta = -0.9$ . Some  $N$ -body simulations face a crucial problem, as they predict that voids should be filled with dwarf galaxies.

In our models, we assume that the real density contrast in voids is the same as the one obtained from galaxy observations.

## 5 THE LEMAÎTRE-TOLMAN MODEL

### 5.1 Formulae and general properties

The L-T model is a spherically symmetric solution of Einstein's equations with a dust source. In comoving and synchronous coordinates, the metric is

$$ds^2 = c^2 dt^2 - \frac{R_{,r}^2(r, t)}{1 + 2E(r)} dr^2 - R^2(t, r) d\Omega^2, \quad (2)$$

where  $d\Omega^2 = d\theta^2 + \sin^2\theta d\phi^2$  and  $E(r)$  is an arbitrary function of  $r$ . Because of the signature  $(+, -, -, -)$ , this function must obey  $E(r) \geq -\frac{1}{2}$ .

The Einstein equations reduce to the following two:

$$\kappa\rho c^2 = \frac{2M_{,r}}{R^2 R_{,r}}, \quad (3)$$

$$\frac{1}{c^2} R_{,t}^2 = 2E + \frac{2M(r)}{R} + \frac{1}{3} \Lambda R^2, \quad (4)$$

where  $M(r)$  is another arbitrary function and  $\kappa = \frac{8\pi G}{c^4}$ .

When  $R_{,r} = 0$  and  $M_{,r} \neq 0$ , the density becomes infinite. This happens when shell crossings occur. Equation (4) is similar to its Newtonian counterpart for a spherical dust distribution:

$$\frac{1}{2} \mathcal{R}_{,t}^2 = \frac{\mathcal{E}}{m} + \frac{GM}{\mathcal{R}},$$

where  $\mathcal{R}$ ,  $\mathcal{E}$  and  $\mathcal{M}$  are respectively the radial coordinate, the energy of the particles and the mass within radius  $\mathcal{R}$  (in Newtonian mechanics, the cosmological constant is not considered). Therefore,  $M(r)c^2/G$  is the mass inside the shell of the radial coordinate  $r$ , and  $E(r)c^2$  is the energy per mass unit.

Equation (4) can be solved by simple integration:

$$\int_0^R \frac{d\tilde{R}}{\sqrt{2E + \frac{2M}{\tilde{R}} + \frac{1}{3}\Lambda\tilde{R}^2}} = c[t - t_B(r)], \quad (5)$$

where  $t_B$  appears as an integration constant and is an arbitrary function of  $r$ . This means that the big bang is not a single event as in the Friedmann models, but occurs at different times for different distances from the origin.

When  $\Lambda = 0$ , the above equation can be solved in parametric form, as follows.

(i) For  $E < 0$ :

$$R = -\frac{M}{2E}(1 - \cos\eta),$$

$$\eta - \sin\eta = \frac{(-2E)^{3/2}}{M} c[t - t_B(r)]. \quad (6)$$

Eliminating  $\eta$ , one can write this as<sup>3</sup>

$$ct_B = ct - \frac{M}{(-2E)^{3/2}} \left[ \arccos\left(1 + 2\frac{ER}{M}\right) - \sqrt{1 - \left(1 + 2\frac{ER}{M}\right)^2} \right]. \quad (7)$$

(ii) For  $E = 0$ :

$$R = \left\{ \frac{9}{2} M c^2 [t - t_B(r)]^2 \right\}^{\frac{1}{3}}. \quad (8)$$

(iii) For  $E > 0$ :

$$R = \frac{M}{2E} (\cosh\eta - 1),$$

$$\sinh\eta - \eta = \frac{(2E)^{3/2}}{M} c[t - t_B(r)]; \quad (9)$$

<sup>3</sup> Equation (7) applies with  $\eta < \pi$ , i.e. in the expansion phase. We do not consider the recollapse phase in this paper.

or equivalently,

$$ct_{\text{B}} = ct - \frac{M}{(2E)^{3/2}} \left[ \sqrt{\left(1 + 2\frac{ER}{M}\right)^2 - 1} - \operatorname{arcosh} \left(1 + 2\frac{ER}{M}\right) \right]. \quad (10)$$

Thus, the evolution of an L–T model is determined by three arbitrary functions:  $E(r)$ ,  $M(r)$  and  $t_{\text{B}}(r)$ . The metric and all the formulae are covariant under arbitrary coordinate transformations of the form  $r = f(r')$ . Using such a transformation, one function can be given a desired form. Therefore the physical initial data for the evolution of the L–T model consist of two arbitrary functions.

## 5.2 The Friedmann limit

The L–T model is a generalization of the Friedmann models and becomes a Friedmann model when the following conditions are fulfilled.

$$(i) \quad t_{\text{B}} = \text{constant}. \quad (11)$$

This constant is usually set to zero.

$$(ii) \quad \frac{|E|^{3/2}}{M} = \text{constant}. \quad (12)$$

In the Friedmann limit, the density distribution is a function of the time coordinate only and is expressed by the formula

$$\kappa\rho c^2 = \frac{6M}{R^3}. \quad (13)$$

The above conditions are invariant under any coordinate transformation. In the class of coordinates used here, one can choose the radial coordinate as

$$R(r, t) = rS(t), \quad (14)$$

where  $S$  is the scale factor of the Friedmann models, and then

$$M(r) = M_0 r^3, \quad E(r) = E_0 r^2. \quad (15)$$

The Friedmann limit is an essential element in our approach. As mentioned above, our model of void formation describes a single void in an expanding Universe. Far away from the origin, the density and velocity distributions tend to the values that they would have in a Friedmann model. The mean sizes of voids presented in the literature are estimated in the Friedmann models (each estimate uses one specific model, but for low redshifts the differences between different models are negligible). Using equation (14) one can identify the areal radius of a void  $R(r_v, t_0)$  with the mean void radius given in the literature.

## 6 BACKGROUND MODELS

The aim of this paper is to describe the formation of voids from initial density and velocity perturbations at the time of last scattering and also to check how the evolution of a void depends on the background model. This requires knowledge of the density and velocity perturbations and also of the age of the Universe at the moment of last scattering. Although not all the background models used here are consistent with observations, even those excluded by observations will clarify some mechanisms responsible for void formation. The astronomical data put limits on the values of some parameters. From the observation of the oldest stars, the lower limit for the age

of the Universe is estimated to be approximately  $12\text{--}14 \times 10^9$  yr (Spergel et al. 2003). From the measurement of the movement of galaxies in clusters and of matter in galaxies, one can estimate the mean matter density. In the critical density units, this value is  $\Omega_{\text{mat}} \sim 0.3$ . Observations of Type Ia supernovae and of the microwave background radiation suggest a non-zero cosmological constant, of approximate value  $\Omega_{\Lambda} \sim 0.73$  (Bennett et al. 2003).

In the following, the subscript  $_{\text{b}}$  indicates a background value,  $_{\text{o}}$  indicates a present-day value and  $_{\text{ls}}$  indicates a value at last scattering.

## 6.1 Background models without cosmological constant

### 6.1.1 The Einstein-de Sitter universe

The Einstein-de Sitter universe is the flat Friedmann model filled with matter and without the cosmological constant. This model can be obtained from the L–T model. From equations (13) and (11) with  $E = 0$ , it follows that the density of the homogeneous background is

$$\rho_{\text{b}} = \frac{6M}{\kappa c^2 R_{\text{b}}^3} = \frac{1}{6\pi G t^2}. \quad (16)$$

Substituting above the critical density obtained from the Hubble constant  $H_0 = 72 \text{ km s}^{-1} \text{ Mpc}^{-1}$  (Bennett et al. 2003), one can obtain that the present age of the Universe is  $9.053 \times 10^9$  yr. The last scattering photons on electrons took place when  $z \approx 1089$  (Bennett et al. 2003). It was not a single event, but a process extended in time. In what follows, it will be assumed that the last scattering took place when  $z = 1089$ . At that instant, the background density was equal to

$$(\rho_{\text{ls}})_{\text{b}} = (\rho_0)_{\text{b}}(1+z)^3, \quad (17)$$

so from equation (16) we obtain that the Universe was 252 000 yr old.

The following quantity is a measure of the velocity:

$$b = \frac{R_{,t}}{cM^{1/3}}. \quad (18)$$

In the flat background this becomes

$$b_{\text{b}} = \frac{(R_{,t})_{\text{b}}}{cM^{1/3}} = \left(\frac{4}{3ct}\right)^{1/3}. \quad (19)$$

### 6.1.2 The hyperbolic background

The hyperbolic background is the  $k < 0$  Friedmann model. The age of the Universe at the moment of last scattering can be calculated using equation (19). In the Friedmann models, the factor  $M/E^{3/2}$  is constant and one can calculate it assuming that the current expansion rate of the homogeneous background is given by the Hubble constant:

$$H_0^2 = \left. \frac{R_{,t}^2}{R^2} \right|_0 = \frac{2Ec^2}{R_0^2} + \frac{2Mc^2}{R_0^3} = \frac{2Ec^2}{R_0^2} + \frac{1}{3}\kappa c^4 \rho_0. \quad (20)$$

From this, one obtains

$$\frac{2E}{M^{2/3}} = \frac{1}{3}\kappa c^2 (\rho_{\text{crit}} - \rho_0) \left(\frac{6}{\kappa\rho_0 c^2}\right)^{2/3}, \quad (21)$$

where  $\rho_{\text{crit}} = 3H_0^2/\kappa c^4$  is the density of a  $k = 0$  Friedmann model. Substituting the above result in the first equation of (9), one obtains

$$\eta_{\text{ls}} = \operatorname{arcosh} \left[ 2 \frac{1 + \Omega_{\text{mat}}}{\Omega_{\text{mat}}(1+z)} \right], \quad (22)$$

where  $\Omega_{\text{mat}} = \rho_0/\rho_{\text{crit}} = \kappa c^4 \rho_0/3H^2$ . From the above formula and from equations (21) and (9), it follows that the age of the Universe with  $\Omega_{\text{mat}} = 0.27$  when  $z = 1089$  is equal to 477 000 yr. The present age is  $11.1 \times 10^9$  yr. In the model with  $\Omega_{\text{mat}} = 0.391$  (this model has a similar present-day velocity to the model with  $\Omega_{\text{mat}} = 0.27$  and  $\Omega_{\Lambda} = 0.73$ ), one can obtain 402 000 yr for the instant of last scattering and  $10.6 \times 10^9$  yr for today. The value of the background density was calculated from equation (17).

The background velocity in the hyperbolic model is

$$b_b = \frac{(R_{,t})_b}{cM^{1/3}} = \sqrt{\frac{2E}{M^{2/3}} + \frac{2M^{1/3}}{R_b}} \\ = \sqrt{\frac{2E}{M^{2/3}} + 2 \left( \frac{1}{6} \kappa \rho_b c^2 \right)^{1/3}}. \quad (23)$$

## 6.2 The elliptic background

The elliptic background is the  $k > 0$  Friedmann model. The procedure is similar to the one above. To calculate the age of the Universe, one must use equation (6) and a value of  $\eta$  of

$$\eta_{\text{ls}} = \arccos \left[ 1 - 2 \frac{\Omega_{\text{mat}} - 1}{\Omega_{\text{mat}}(1+z)} \right].$$

The age of the Universe in the model with  $\Omega_{\text{mat}} = 11$  is 76 000 yr at last scattering and  $4.6 \times 10^9$  yr today.

## 6.3 Background models with the cosmological constant

### 6.3.1 The flat background

When  $E = 0$ , equation (5) can be solved explicitly:

$$\int_0^R dR' \frac{1}{\sqrt{\frac{2M}{R'} + \frac{1}{3}\Lambda R'^2}} \\ = \sqrt{\frac{4}{3\Lambda}} \operatorname{ar} \coth \left( \frac{3}{\Lambda} \sqrt{\frac{2M}{R'} + \frac{\Lambda}{3}} \right) \\ = c(t - t_B); \quad (24)$$

or equivalently,

$$R^3 = \frac{6M}{\Lambda} \sinh^2 \left( ct \sqrt{\frac{3\Lambda}{4}} \right). \quad (25)$$

It follows that the background density is

$$\kappa c^2 \rho_b = \frac{\Lambda}{\sinh^2 \left( ct \sqrt{\frac{3\Lambda}{4}} \right)}. \quad (26)$$

The age of the Universe can be calculated from the formula given above. Substituting the values suggested by astronomical observations,  $\Omega_{\text{mat}} = 0.27$  and  $\Omega_{\Lambda} = \frac{\Lambda c^2}{3H_0^2} = 0.73$ , we obtain that the density is equal to the critical density, the Universe is  $13.48 \times 10^9$  yr old today, while at the moment of last scattering the age of the Universe was 484 000 yr.

The background velocity in the flat Universe with the cosmological constant is given by the formula

$$b_b = \frac{(R_{,t})_b}{cM^{1/3}} = \frac{2}{3} \left( \frac{6}{\kappa c^2 \rho_b} \right)^{1/3} \sqrt{\frac{3\Lambda}{4}} \coth^2 \left( ct \sqrt{\frac{3\Lambda}{4}} \right). \quad (27)$$

**Table 2.** The age of the Universe at the present epoch and at the moment of last scattering.

Model	Present age of the Universe (yr)	Age at last scattering (yr)
$\Omega_{\text{mat}} = 1, \Omega_{\Lambda} = 0$	$9.053 \times 10^9$	$252 \times 10^3$
$\Omega_{\text{mat}} = 0.27, \Omega_{\Lambda} = 0$	$11.1 \times 10^9$	$477 \times 10^3$
$\Omega_{\text{mat}} = 0.391, \Omega_{\Lambda} = 0$	$10.6 \times 10^9$	$402 \times 10^3$
$\Omega_{\text{mat}} = 11, \Omega_{\Lambda} = 0$	$4.6 \times 10^9$	$76 \times 10^3$
$\Omega_{\text{mat}} = 0.27, \Omega_{\Lambda} = 0.73$	$13.48 \times 10^9$	$484 \times 10^3$
$\Omega_{\text{mat}} = 0.27, \Omega_{\Lambda} = 1.64$	$32.46 \times 10^9$	$485 \times 10^3$

### 6.3.2 Non-flat background models

We follow an analogous procedure to the  $\Lambda = 0$  case and calculate

$$\frac{2E}{M^{2/3}} = \frac{1}{3} \kappa \rho_{\text{crit}} c^2 (1 - \Omega_{\text{mat}} - \Omega_{\Lambda}) \left( \frac{6}{\kappa \rho_b c^2} \right)^{2/3}, \quad (28)$$

where  $\Omega_{\Lambda} = (\Lambda/\kappa c^2)/\rho_{\text{crit}} = \Lambda c^2/3H^2$ . When  $E \neq 0$ , equation (5) does not have an analytic solution. Let us denote

$$\frac{R_b}{M^{1/3}} = a, \quad \frac{2E}{M^{2/3}} = \alpha,$$

then equation (5) can be written

$$\int_0^a \frac{dx}{\sqrt{\alpha + \frac{2}{x} + \frac{1}{3}\Lambda x^2}} = ct. \quad (29)$$

In the model with  $\Omega_{\text{mat}} = 0.27$  and  $\Omega_{\Lambda} = 1.64$ , one finds that the age of the Universe at the moment of decoupling was 485 000 yr and at present it is  $32.46 \times 10^9$  yr. The background velocity is

$$b_b = \frac{(R_{,t})_b}{cM^{1/3}} = \sqrt{\frac{2E}{M^{2/3}} + \frac{2M^{1/3}}{R_b} + \frac{1}{3}\Lambda \frac{R_b^2}{M^{2/3}}} \\ = \sqrt{\frac{2E}{M^{2/3}} + 2 \left( \frac{1}{6} \kappa \rho_b c^2 \right)^{1/3} + \frac{1}{3}\Lambda \left( \frac{6}{\kappa \rho_b c^2} \right)^{2/3}}. \quad (30)$$

The parameters of the various background models are summarized in Table 2.

## 7 PERTURBATIONS AT THE MOMENT OF LAST SCATTERING

The microwave background radiation is a relic from the epoch when the Universe was young and hot. When the temperature of the Universe dropped below 3000 K, the free path of photons became comparable to the Hubble radius and radiation stopped interacting with matter. Consequently, an analysis of this radiation can give us information about the state of matter at that moment. The spectrum of the cosmic microwave background (CMB) is the spectrum of the blackbody with the mean temperature of  $T \approx 2.725$  K (Mather et al. 1999). More precise observations measure the fluctuations with amplitude  $\delta T/T \sim 10^{-5}$ . These are related to the density fluctuations at last scattering. Unfortunately, this relation is complicated: one must take into account several effects.

### 7.1 Linear and angular diameters

The observations of the microwave background radiation measure differences in temperature between two points of the celestial sphere. The angular resolution of the instruments is not high. The Wilkinson Microwave Anisotropy Probe satellite (*WMAP*) measures

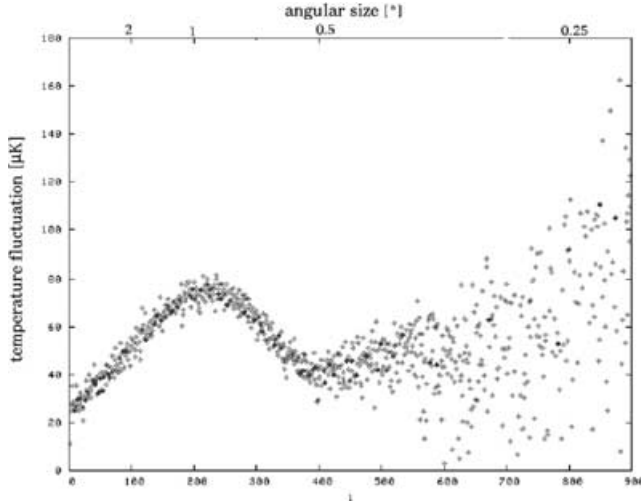


**Figure 2.** The temperature fluctuations ( $\Delta T$ ) measured by *WMAP* (based on data from <http://lambda.gsfc.nasa.gov/product/map/>).

the radiation in five different ranges and, depending on the range, has the resolution from  $0^{\circ}.82$  to  $0^{\circ}.21$  (Bennett et al. 2003). The results of the temperature measurement are presented in Fig. 2.

The following question arises: what are the linear diameters of the regions that *WMAP* can still see as separate? Also, is this resolution sufficient to observe the regions that evolved into the currently observed voids?

The linear diameters can be estimated using the scale law of the Friedmann models:

$$\frac{L_0}{L_{\text{dec}}} = \frac{\chi(r)S_0}{\chi(r)S_{\text{dec}}} = 1 + z, \quad (31)$$

where  $\chi(r)$  is the distance in the space  $t = \text{const}$ ,

$$\chi(r) := [1/S(t)] \int_0^r g_{rr}(t, r') dr'. \quad (32)$$

These diameters are related to the angular diameters:

$$L = D\Delta\theta, \quad (33)$$

where  $D$  is the angular distance; in the Friedmann models, it is determined by

$$D = \frac{S_0}{1+z} \mathcal{F}(d), \quad (34)$$

where

$$\mathcal{F}(d) = \begin{cases} \sin(d), & \text{when } \Omega_{\text{mat}} + \Omega_{\Lambda} > 1 \\ d, & \text{when } \Omega_{\text{mat}} + \Omega_{\Lambda} = 1 \\ \sinh(d), & \text{when } \Omega_{\text{mat}} + \Omega_{\Lambda} < 1 \end{cases} \quad (35)$$

and  $d$  is given by the formula

$$d = \frac{c}{H_0 S_0} \int_0^z dz' \frac{1}{\sqrt{\Omega_c(1+z')^2 + \Omega_{\text{mat}}(1+z')^3 + \Omega_{\Lambda}}}, \quad (36)$$

where  $\Omega_c = 1 - \Omega_{\text{mat}} - \Omega_{\Lambda}$ . Assuming that the moment of last scattering was when  $z = 1089$  and that the mean void diameter is  $25 h^{-1}$  Mpc, for different models one obtains the results shown in Table 3.

Comparing data from Table 3 with Fig. 2, one sees that the resolution of the *WMAP* instruments is not sufficient to make direct measurements of the temperature fluctuations in the regions that became voids.

**Table 3.** Angular diameters of the pre-void region.

Model	$\Delta\theta$
$\Omega_{\text{mat}} = 1, \Omega_{\Lambda} = 0$	$0^{\circ}.246$
$\Omega_{\text{mat}} = 0.27, \Omega_{\Lambda} = 0$	$0^{\circ}.071$
$\Omega_{\text{mat}} = 0.27, \Omega_{\Lambda} = 0.73$	$0^{\circ}.143$

## 7.2 Initial fluctuations

As the starting point of further considerations, we need a rough estimate of the initial conditions. The procedure for estimating the density fluctuations from the observed temperature fluctuations is complicated. The main contributions to the observed temperature perturbation are from the intrinsic temperature fluctuations of the emitting fluid, the frequency shift as light emerges from a fluctuation in the gravitational potential (Sachs–Wolfe effect), and from the Doppler effect (motion of the emitter). The moment of last scattering also depends on the cosmological background model, but for different models the differences are negligible. For completeness, one should take into account what happened to the radiation on the way to the observer: the integrated Sachs–Wolfe effect (the effect of gravitational perturbations along the line of sight), the Rees–Sciama effect (the influence of changes of the gravitational potential with time), the Sunyaev–Zeldovich effect (radiation interacting with galaxy clusters) and the non-linear consequences of the photons travelling in an inhomogeneous space.

It is found (e.g. Padmanabhan 1996) that the intrinsic temperature fluctuations obey  $(\Delta T/T)_{\text{intrinsic}} \sim \Delta\rho/3\rho$ . The magnitude of velocity perturbations is usually not given.<sup>4</sup> Fluctuations in the fluid motion of magnitude  $\Delta V$  (away from uniform expansion) must contribute a Doppler term  $(\Delta T/T)_{\text{Doppler}} = \Delta V/c$ , so observations of  $\Delta T/T \leq 10^{-5}$  put an upper limit of  $10^{-5} c$  on  $\Delta V$ . On the other hand, because the fluctuations are acoustic oscillations, the three contributions to  $(\Delta T/T)_{\text{observed}}$  must be of comparable magnitude,  $(\Delta T/T)_{\text{intrinsic}} \sim \Phi/3 \sim \Delta V/c$ . Indeed, for an oscillating fluid with a relativistic equation of state ( $\partial p/\partial\rho = c^2$ ), we must have  $\Delta V \sim c\Delta\rho/3\rho$ .

However, the major problem is not with calculations, but with the data. The present data are available for scales larger than the scale of a single void and all these calculations must rely on extrapolations.

The *WMAP* data that were used as the source for Fig. 2 have such a large scatter for scales around  $0^{\circ}.2$  that the temperature fluctuation could be anything from  $10^{-4}$  to  $10^{-6}$ . Using the extrapolation proposed by the *WMAP* team, one would get  $\Delta T/T \approx 2 \times 10^{-5}$ .

To estimate  $v = \Delta V/V_b = \Delta b/b_b$  for a present-day scale of  $L_0 = 12$  Mpc, we write  $L = L_0/(1+z)$ ,  $H = H_0(1+z)^{1/n}$ ,  $V_b = LH$  and  $n = 2/3$  for an Einstein–de Sitter model. Thus we find, for  $H_0 = 72 \text{ km s}^{-1} \text{ Mpc}^{-1}$  and  $z = 1089$ , that

$$v \approx 2 \times 10^{-4}. \quad (37)$$

## 8 FORMATION OF VOIDS

In this section, we will check whether it is possible to evolve the voids from a small initial density and velocity perturbation imposed

<sup>4</sup> It is commonly stated by specialists that  $\Delta V/c \sim 10^{-5}$  but we have not been guided to a reference that says this or something equivalent.

on a homogeneous background. We will also check what is the influence on the structure formation of the following factors:

- (i) the shape and the amplitude of the initial perturbations;
- (ii) the evolution time;
- (iii) the expansion rate; and
- (iv) the outflow of mass from central parts of the void.

The evolution of the void will be calculated with six different background models. Some of these models, especially the elliptic ones with and without cosmological constant, are inconsistent with the observations. These are used not in order to obtain a model of the observed Universe, but to check which of the factors listed above are more important in the process of void formation. For comparing the various models, let us assume that the initial conditions are independent of the background model.

To determine the evolution of the L–T model, one needs to know two functions. In this paper, these functions will be the initial density and velocity distributions. This is not the only method to specify the evolution in the L–T model. The evolution can be determined also by giving the initial and the final density profiles (Kraśniński & Hellaby 2002) or the initial velocity distribution and the final density distribution (Kraśniński & Hellaby 2004).<sup>5</sup>

## 8.1 The algorithm

The computer algorithm used to calculate the evolution of a void was written in FORTRAN and consisted of the following steps. Numerical methods are from Press et al. (1986) and Pang (1997).

(i) The initial time  $t_i$  was chosen to be the time of last scattering. This moment was calculated as described in Section 6.3.2 Equation (29) was integrated using Bode's rule with the step of value  $10^{-6} \times [6/(\kappa \rho_{cr} c^2 \Omega_{mat})]^{1/3}$ . The homogeneous background density and velocity were calculated from equations (17) and (30) as described in Section 6.3.2

(ii) The initial density and velocity fluctuations, imposed on this homogeneous background, were defined by functions of radius  $\ell$ ,

$$\delta(\ell) \text{ and } v(\ell),$$

as listed in Tables 4 and 5, and the actual density and velocity followed from

$$\rho_i(\ell) = (\rho_b)_i [1 + \delta(\ell)] \text{ and } b(\ell) = (b_b)_i [1 + v(\ell)],$$

with  $\rho$  measured in units of  $10^{45} M_\odot \text{ kpc}^{-3}$  and  $b$  in  $\text{kpc}^{-1/3}$ . The parameter  $\ell$  is defined as the areal radius at the moment of last scattering, measured in kiloparsecs, and is also used for the radial coordinate, i.e.

$$r = \ell = R_i/d = R(r, t_i)/d,$$

where  $d = 1 \text{ kpc}$ .

(iii) Then the mass inside the shell of radius  $R_i$ , measured in kiloparsecs, was calculated by integrating equation (3):

$$M(\ell) - M(0) = \frac{\kappa c^2}{2} \int_{\ell_{\min}}^{\ell} \rho_i(\ell') \ell'^2 d\ell' \Big|_{t=t_{ls}}. \quad (38)$$

Because the density distribution has no singularities or zeros over extended regions, it was assumed that  $\ell_{\min} = 0$  and  $M = 0$  at  $\ell = 0$ .

The integration was done using Bode's rule, with step size 2.5 pc.

(iv)  $E$  was calculated from  $R_i$ ,  $V = (R_{,i})_i$ ,  $M$  and a chosen  $\Lambda$  value, using equation (4).

(v) Then  $t_B$  was calculated from equation (5) using Simpson integration, with step size  $10^{-5} \ell$ .

(vi) Once  $M$ ,  $E$  and  $t_B$  are known, the state of the L–T model can be calculated for any instant. Solving equation (4) with the second-order Runge–Kutta method for  $R(t, \ell)$  along each constant  $\ell$  worldline, we calculated the value of  $R(t, \ell)$  and  $R_{,i}(t, \ell)$  up to the present epoch. The time step was  $5 \times 10^5 \text{ yr}$ .

(vii) The density  $\rho(t, \ell)$  was then found from equation (3) using the five-points differentiating formula. The adjusted differences between adjacent worldlines, used in estimating derivatives, was 10 pc.

(viii) The density contrasts presented in Section 8.2 were estimated from equation (39).

## 8.2 The void models

### 8.2.1 Initial perturbations of homogeneity

Because of a lack of precise observational data, it is not possible to calculate the exact profile of the initial density and velocity perturbations. From the measurements of the microwave background radiation, one can estimate only the amplitudes of these profiles. It can be intuitively expected that the region that in the future would become a void should have, at the initial instant, a minimum of density and a maximum of velocity at the centre.<sup>6</sup>

The chosen initial density and velocity distributions fulfilling the above conditions are presented in Fig. 3. These profiles conform to the amplitudes estimated in Section 7.2. They were defined by the functions presented in Tables 4 and 5.<sup>7</sup>

From the current observations, only the average density contrast is known. For the purpose of comparing our results with the observational data (Fig. 1), the results shown in Fig. 4 (and also the figures showing the final density contrast in what follows) do not present the real density contrast, but the average one, i.e.

$$\delta = \frac{\langle \rho \rangle}{\bar{\rho}} - 1, \quad (39)$$

where  $\bar{\rho}$  is the present background density

$$\langle \rho \rangle = \frac{3Mc^2}{4\pi GR^3}. \quad (40)$$

Unfortunately there are no astronomical data for the current velocity distribution in the void. It is more practical to measure the expansion rate by the equivalent of the Hubble parameter ( $R_{,i}/R$ ). The results are presented in Fig. 4.

Fig. 5 shows the redistribution of mass resulting from void formation. Curve 0 is the function  $M(R)$  at the initial time  $t = t_{ls}$  [i.e.  $M(r)$  versus  $R(r, t_{ls})$ ] and the other curves show the calculated  $M(R)$  at the present time,  $t = t_0$ , for different background models.

Curve 6 in Fig. 4 is truncated. At the cut-off point, a shell crossing occurs: the inner shells catch up with the outer shells. This results in a singularity that probably does not occur in the real Universe.

<sup>6</sup> However, see the papers by Mustapha & Hellaby (2001) and by Kraśniński & Hellaby (2002): maxima and minima can be reversed during evolution, and it is not at all necessary that a void begins with a minimum of density at the centre.

<sup>7</sup> The form of these initial density and velocity distributions is a result of consecutive adjustments made in order to test the influence on void formation of the various factors mentioned at the beginning of this section.

<sup>5</sup> The numerical examples in those papers used the present day for the final time.

**Table 4.** The initial density perturbations used in the runs. All the values in the table are dimensionless and the distance parameter is the areal radius in kiloparsecs  $\ell = R_i/1$  kpc. Note that the output figures depend on the initial perturbation in both density and velocity.

Section	Model	Density perturbation	Parameters	Graph	Output
8.2.1	1–6	$\delta_{\text{INIT}}(\ell) = A(b \arctan c - d\ell - fe^{-g^2} - e^{-h^2} - ie^{-j^2})k$	$A = 1.1 \times 10^{-5}$ $b = 4$ $c = 0.16\ell - 2.2$ $d = 1/7$ $f = 0.5$ $g = (\ell - 7)/6$ $h = (\ell - 9)/7$ $i = 1.4$ $j = (\ell - 11)/3$ $k = 1/(1 + 0.03\ell)$	Fig. 3	Figs 4, 5
8.2.2	1–6	$\delta = \delta_{\text{INIT}}(\ell)$		Fig. 3	Fig. 6
8.2.3	1–6	$\delta = 0$			Similar to Figs 4, 5
8.2.4	1–6	$\delta_{\text{AMP}}(\ell) = A(b \arctan c - d\ell - fe^{-g^2} - e^{-h^2} - e^{-j^2})k$	$A = 7.5 \times 10^{-4}$ $b = 4$ $c = 0.08\ell - 1.1$ $d = 1/11$ $f = 0.4$ $g = \ell/4$ $h = (\ell - 2)/7$ $j = (\ell - 4)/3$ $k = 1/(1 + 0.03\ell)$		Fig. 7
8.2.5	1, 2, 3	$\delta_{1,2,3}(\ell) = 100 \delta_{\text{INIT}}(\ell)$		Fig. 8	Figs 9, 10, 11
8.2.5	4	$\delta_4(\ell) = 2 \delta_{1,2,3}(\ell)$		Fig. 8	Figs 9, 10, 11
10.2.1	both	$\delta_{\text{RAD}}(\ell) = A(b \arctan c - d\ell - fe^{-g^2} - e^{-h^2} - e^{-j^2})k$	$A = 7.5 \times 10^{-4}$ $b = 4$ $c = 0.08\ell - 1.1$ $d = 1/11$ $f = 0.4$ $g = (\ell - 2)/4$ $h = (\ell - 4)/7$ $j = (\ell - 6)/3$ $k = 1/(1 + 0.03\ell)$		Fig. 16

Before it happens, the gradient of pressure would become significant and the L–T model would become invalid.

From the figures presented above, some initial conclusions can be made. One can say that the current depth of the void depends on the amount of mass redistribution, i.e. the mass outflow. This outflow depends on the expansion rate and on the age of the void. The major influence on the structure formation is from the shell expansion.

In models 4 and 5, the expansion rate is bigger than in models 1–3, and the final density contrast in models 4 and 5 is much more negative than in models 1–3, even though the age of the Universe in these models is much lower.

Unfortunately, models 1–5 cannot recover the observed density contrast of the voids of today. The proper depth can be obtained only in model 6, where the age of the Universe is significantly larger.

The age of the void (in limits estimated by the various astronomical observations) is of lesser importance, compared with the expansion rate. In models 2 and 3, the expansion of the shells is similar and the final density contrast in model 3 is lower due to the time available for evolution being  $2 \times 10^9$  yr longer.

We now check how big the influence of the initial shape of the density and velocity perturbations is.

### 8.2.2 Homogeneous velocity profile

For this case, the initial density profile  $\delta$  is as in Fig. 3, while the initial velocity profile is  $v = 0$ . The explicit formulae for these profiles are presented in Tables 4 and 5.

The results shown in Fig. 6 seem to be surprising. The mass redistribution is almost the same in all the models (except model 6), the diameters are similar, but the current density profiles are different. In this case, a second factor responsible for the void formation is seen, which is the faster expansion rate. The faster expansion of the void compared with the homogeneous background causes that the difference between the density in the central regions of the void and the density in the background increases with time, even when the mass of the shell inside the region of  $R(t, r)$  is not changing very much. Consequently, in the models with a higher expansion rate, the density contrast is most negative.



**Table 5.** The initial velocity perturbations used in the runs. All the values in the table are dimensionless and the distance parameter is the areal radius in kiloparsecs  $\ell = R_i/1$  kpc. Note that the output figures depend on the initial perturbation in both density and velocity.

Section	Model	Velocity perturbation	Parameters	Graph	Output
8.2.1	1-6	$v_{\text{INIT}}(\ell) = A(b \arctan c - d\ell - fe^{-g^2} - e^{-h^2} - ie^{-j^2})k$	$A = -4 \times 10^{-5}$ $b = 4$ $c = 0.16\ell - 2.2$ $d = 1/7$ $f = 0.5$ $g = (\ell - 7)/6$ $h = (\ell - 9)/7$ $i = 1.4$ $j = (\ell - 11)/3$ $k = 1/(1 + 0.03\ell)$	Fig. 3	Figs 4, 5
8.2.2	1-6	$v = 0$			Fig. 6
8.2.3	1-6	$v = v_{\text{INIT}}(\ell)$		Fig. 3	Similar to Figs 4, 5
8.2.4	1-6	$v_{\text{AMP}}(\ell) = A(b \arctan c - d\ell - fe^{-g^2} - e^{-h^2} - e^{-j^2})k$	$A = -7.5 \times 10^{-4}$ $b = 4$ $c = 0.08\ell - 1.1$ $d = 1/11$ $f = 0.4$ $g = \ell/4$ $h = (\ell - 2)/7$ $j = (\ell - 4)/3$ $k = 1/(1 + 0.03\ell)$		Fig. 7
8.2.5	1	$v_1(\ell) = 37.5 v_{\text{INIT}}(\ell)$		Fig. 8	Figs 9, 10, 11
8.2.5	2,4	$v_{2,4}(\ell) = A(b \arctan c - d\ell - fe^{-g^2} - e^{-h^2} - e^{-j^2} - me^{-n^2})k + p$	$A = -3.5 \times 10^{-3}$ $b = 4$ $c = 0.02\ell - 0.02$ $d = 1/11$ $f = 0.7$ $g = \ell$ $h = (\ell - 1)/7$ $j = (\ell - 3)/3$ $m = 1.225$ $n = (\ell - 39)/12$ $k = 1/(1 + 0.03\ell)$ $p = 5 \times 10^{-4}$	Fig. 8	Figs 9, 10, 11
8.2.5	3	$v_3(\ell) = A(b \arctan c - d\ell - fe^{-g^2} - e^{-h^2} - e^{-j^2} - me^{-n^2})k + p$	$A = -3.5 \times 10^{-3}$ $b = 4$ $c = 0.02\ell - 0.02$ $d = 1/11$ $f = 0.7$ $g = \ell$ $h = (\ell - 1)/7$ $j = (\ell - 3)/3$ $m = 0.7$ $n = (\ell - 39)/12$ $k = 1/(1 + 0.03\ell)$ $p = 5 \times 10^{-4}$	Fig. 8	Figs 9, 10, 11
10.2.1	both	$v_{\text{RAD}}(\ell) = A(b \arctan c - d\ell - fe^{-g^2} - e^{-h^2} - e^{-j^2})k$	$A = -7.5 \times 10^{-4}$ $b = 4$ $c = 0.08\ell - 1.1$ $d = 1/11$ $f = 0.4$ $g = (\ell - 2)/4$ $h = (\ell - 4)/7$ $j = (\ell - 6)/3$ $k = 1/(1 + 0.03\ell)$		Fig. 16

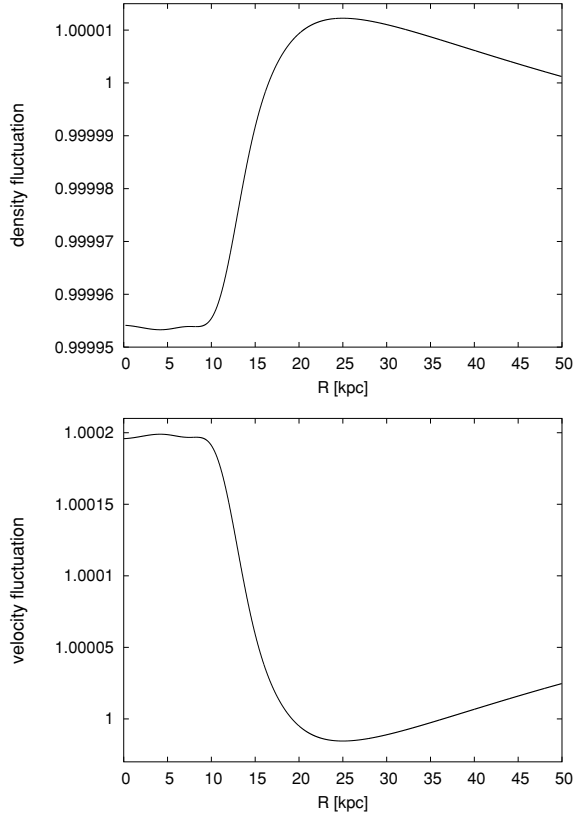


**Figure 3.** The initial density (upper) and velocity (lower) perturbations for data discussed in Section 8.2.1

### 8.2.3 Homogeneous density profile

In contrast to the above, we now set the initial density profile to  $\delta = 0$ , while the initial velocity profile,  $v$ , is as in Fig. 3. The explicit formulae for the profiles are presented in Tables 4 and 5.

The final results are not very different from the one shown in Fig. 4. This proves that the velocity distribution in the formation of voids is very significant, while the density distribution is of lesser importance.

### 8.2.4 Amplitude

In this subsection, the amplitude of the initial fluctuations is increased compared with the one used in Section 8.2.1 and is  $4 \times 10^{-3}$ . The profiles of the initial perturbations are presented in Tables 3 and 4, and the final results in Fig. 7.

The increased amplitude of the initial perturbations results in a void with a higher negative density contrast. To obtain a density contrast near  $\delta \sim -0.9$ , we needed to increase the amplitude of the initial density profile more than 70 times and the amplitude of the velocity profile 20 times, compared with the values estimated from CMB fluctuations. Even so, the value  $\delta = -0.94$  of the density contrast in the void was not reached, except in the two non-realistic background models. In model 4, the minimum value is  $-0.908$  and, in model 3, it is  $-0.873$ . Unfortunately, increasing the amplitude leads to a shell crossing singularity in some models.

### 8.2.5 Observation and a model: a crosscheck

In the previous sections, we had problems generating voids from small initial density and velocity fluctuations. The only alternative

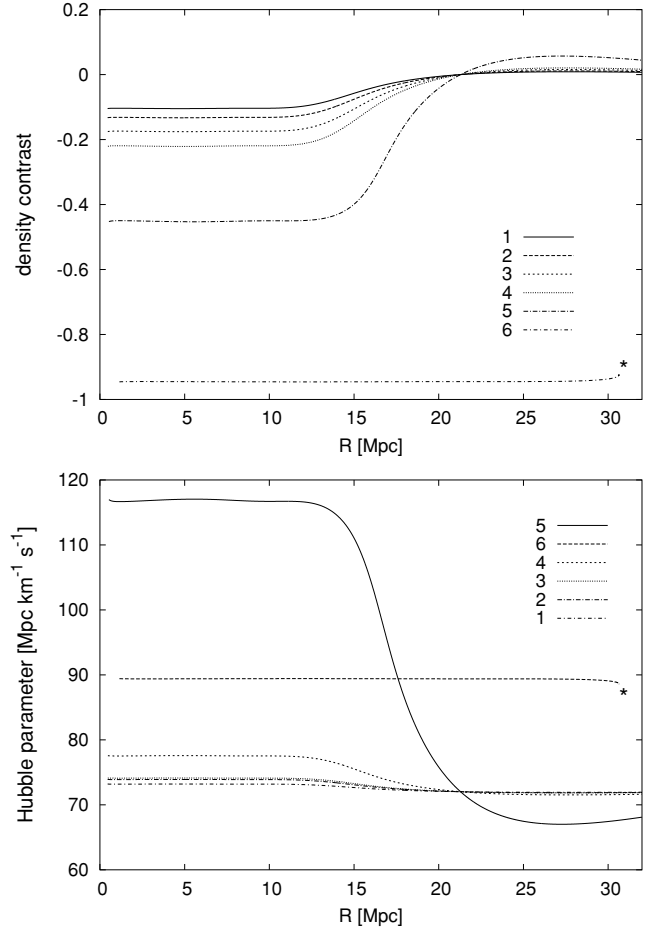


**Figure 4.** The current density contrast and the Hubble parameter for data discussed in Section 8.2.1, in six different background models: 1,  $\Omega_{\text{mat}} = 0.27$ ,  $\Omega_{\Lambda} = 0$ ; 2,  $\Omega_{\text{mat}} = 0.39$ ,  $\Omega_{\Lambda} = 0$ ; 3,  $\Omega_{\text{mat}} = 0.27$ ,  $\Omega_{\Lambda} = 0.73$ ; 4,  $\Omega_{\text{mat}} = 1$ ,  $\Omega_{\Lambda} = 0$ ; 5,  $\Omega_{\text{mat}} = 11$ ,  $\Omega_{\Lambda} = 0$ ; 6,  $\Omega_{\text{mat}} = 0.27$ ,  $\Omega_{\Lambda} = 1.64$ . Shell crossing denoted by \*.

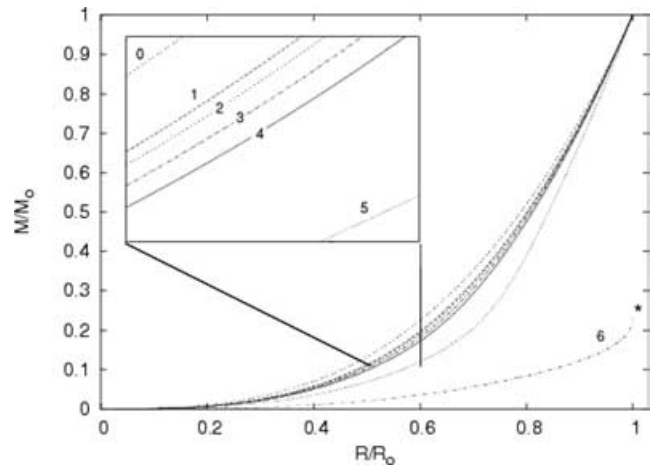


**Figure 5.** The mass redistribution for data discussed in Section 8.2.1  $R_0$  is the smallest  $R$  value at which the density takes the background value.  $M_0$  is the mass inside the shell of areal radius  $R_0$ . 0, the initial condition; other labels as in Fig. 4.

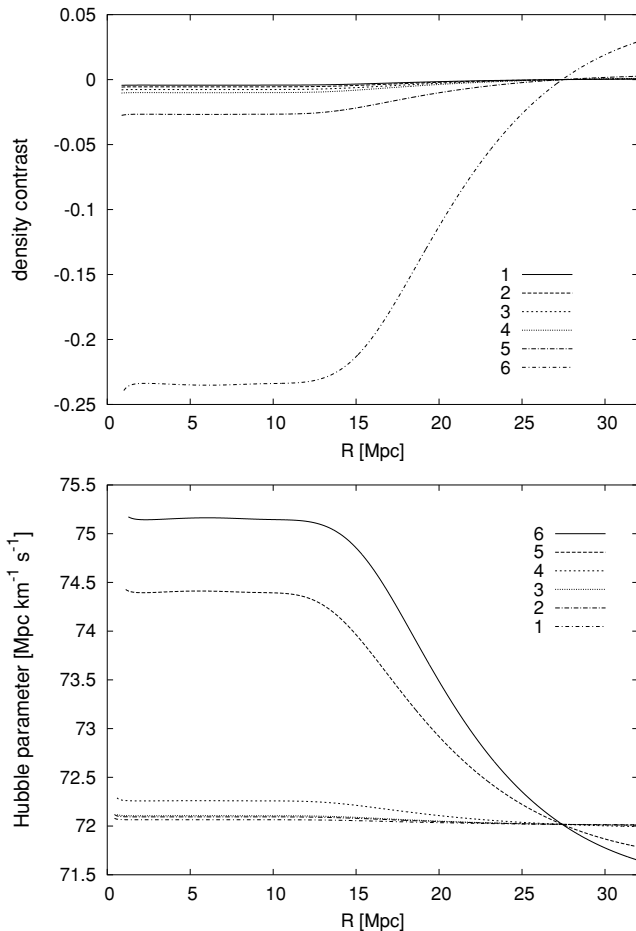


**Figure 6.** The current density contrast and the Hubble parameter for the flat initial velocity profile in different background models. Labels as in Fig. 4.

was to use a background model with an extremely large age of the Universe (inconsistent with limits estimated by the various astronomical observations).

In this subsection, we will try to choose the initial profiles that lead to the best fit with observational data. We focus only on one background model, preferred by the astronomical observations, which is  $\Omega_{\text{mat}} = 0.27$  and  $\Omega_{\Lambda} = 0.73$ . It should be noted that the difference between void evolution in this model and in the Einstein-de Sitter model is not big, so the problem of void formation is in the initial conditions rather than in the background model.

So far none of the results obtained has recovered the observational data, presented in Fig. 1. This figure presents the density profile of the void with very smooth edges. Unfortunately, this profile does not reach to regions where the density is higher than the background density and where the superclusters of galaxies would be found. The mean value of the density contrast inside the void is  $\delta \sim -0.94$ . The density contrasts of the voids obtained so far have been too shallow or had steep edges.

The initial fluctuations are presented in Fig. 8. The profiles are presented in Tables 4 and 5. The results are shown in Figs 9 and 10. Model 2 has both a proper density contrast and smooth edges. The conclusion from numerical experiments with different shapes of the initial profiles is that a model of a void consistent with observational data (with the value of density contrast less than  $\delta = -0.94$ , smooth edges and high density in the surrounding regions) is very hard to obtain within the L–T model, without the occurrence of a shell

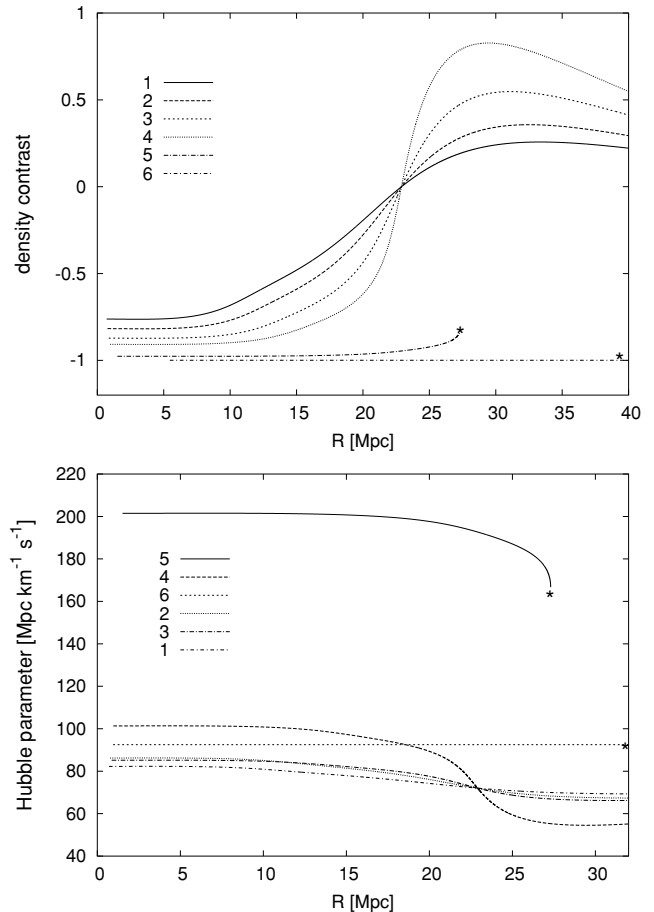


**Figure 7.** The current density contrast and the Hubble parameter for the initial data with higher amplitude of density and velocity perturbation, in six different background models. Labels as in Fig. 4.

crossing singularity. The final state of model 2 was very close to this singularity and in model 4 a shell crossing occurred.

The main factor responsible for void formation is the velocity perturbation, with an amplitude of  $\sim 8 \times 10^{-3}$ , near the centre, and dropping below zero in the outer regions (model 3 did not fulfill this condition). The density fluctuation is of lesser importance. The models 1–3 had the same initial density fluctuations and in model 4 the amplitude was 2 times greater. In spite of these differences, the final results differ only in shape and not in the depth of the final density contrast.

In simulations with higher values of background density, the initial velocity and density perturbation needed to obtain similar final results are smaller (see Section 8.2.4).

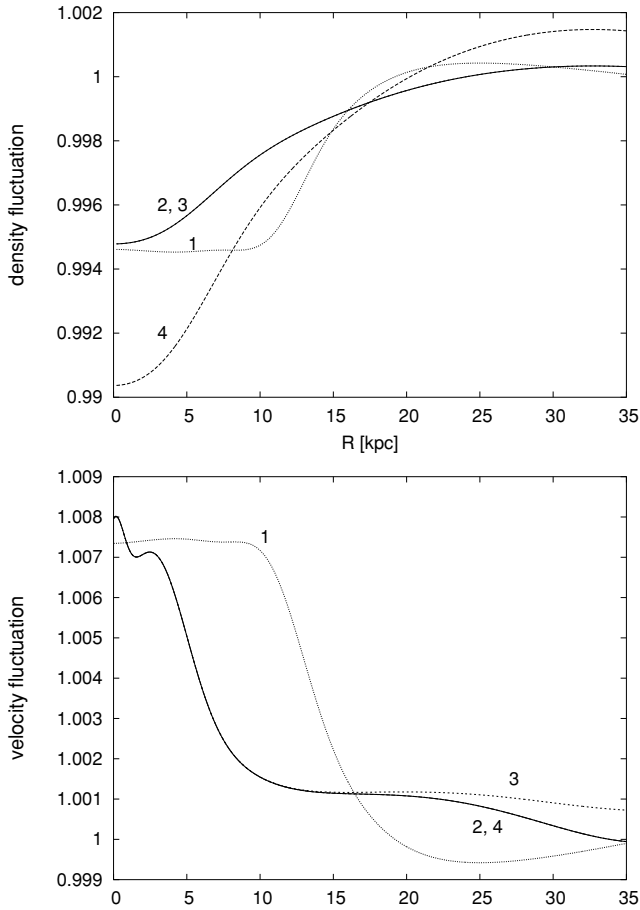
## 9 EVOLUTION

As it can be seen from Fig. 11, model 2 fits the observational data the best.

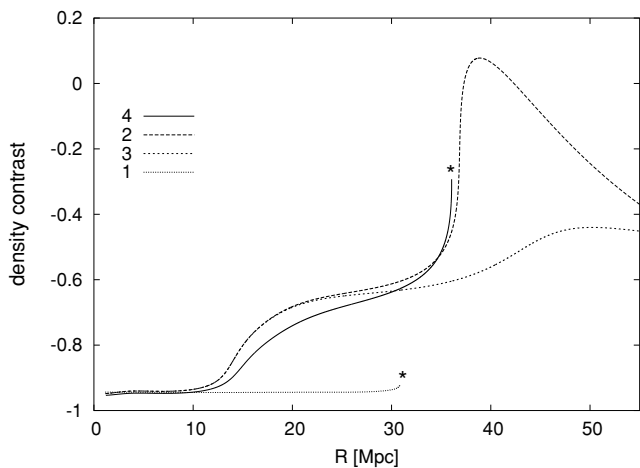
Let us take a closer look at the evolution of model 2.

Fig. 12 shows the density distribution in eight different moments of time. In this section, the figures do not present the density contrast, but the real density distribution calculated from equation (3).

Figs 13–15 show respectively the functions  $M(R)$ ,  $t_B(R)$  and  $E(R)$ , where  $R$  is the areal radius at the initial instant (curves 0) and at the final instant (curves 1). The pictures demonstrate the evolution of the structure: in the expanding void, mass moves outwards.



**Figure 8.** The initial density (upper) and velocity (lower) perturbations for the results presented in Figs 9 and 10.



**Figure 9.** The current density contrast for the models discussed in Section 8.2.5

As one can see from Fig. 14, the difference in the value of the bang time function between outer and central regions of the void is of the order of hundreds of years. This is negligible compared with the age of the Universe, which at the moment of last scattering was of the order of  $10^5$  yr.

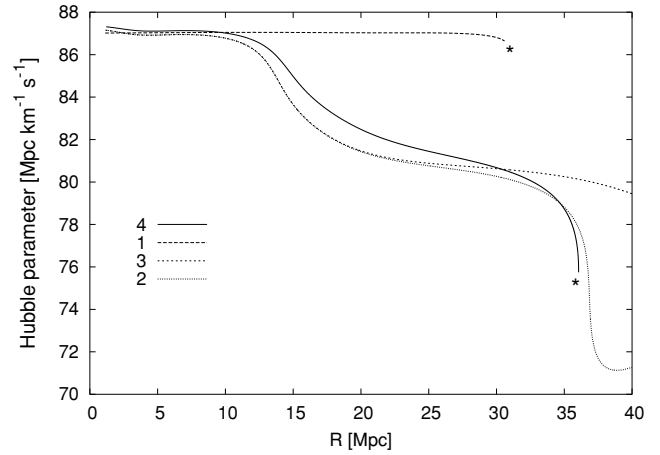


**Figure 10.** The Hubble parameter for the models discussed in Section 8.2.5

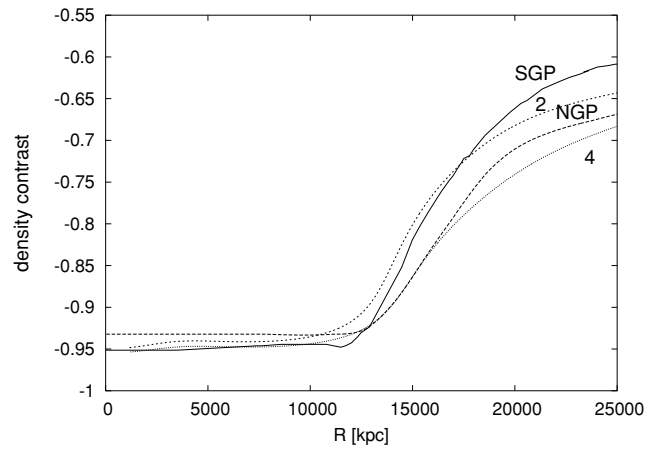


**Figure 11.** Comparison of the curves from Fig. 9 (2, 4) with the observed density contrast from Hoyle & Vogeley (2004; SGP and NGP).

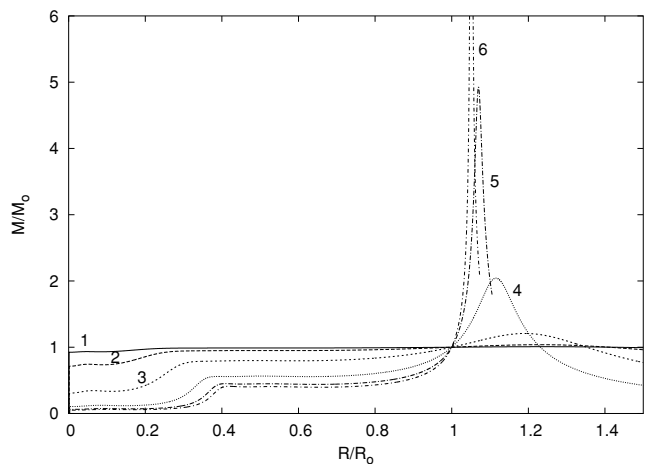


**Figure 12.** The evolution of the density distribution in a void for the age of the Universe: 10 (No. 1), 100 (No. 2) million years and 1 (No. 3), 5 (No. 4), 10 (No. 5) billion years after the big bang, and the current (No. 6) profile of density distribution for the model discussed in Section 9.  $R_0$  is the point at which the density takes the background value for the first time.

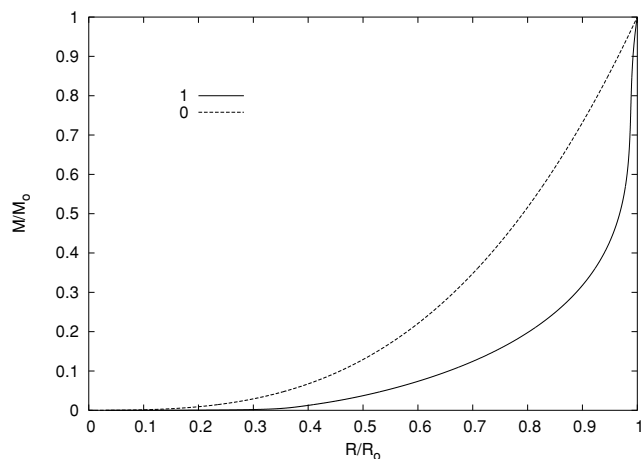


**Figure 13.** The mass redistribution for data discussed in Section 9.  $R_0$  is the point at which the density takes the background value for the first time.  $M_0$  is the mass inside the shell of areal radius  $R_0$ . Curve 0 is the function  $M(R)$  with  $R$  and  $R_0$  taken at  $t_1$ , curve 1 is the function  $M(R)$  with  $R$  and  $R_0$  taken at time  $t_2$ .

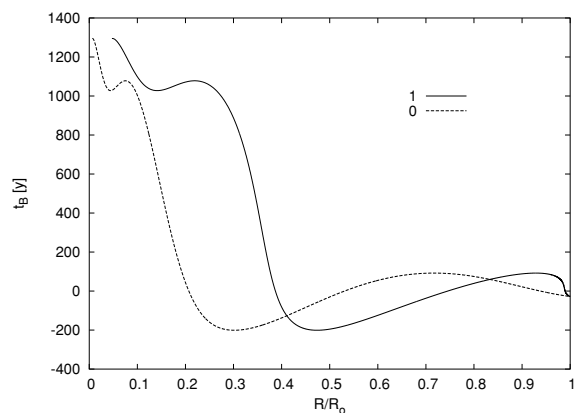


**Figure 14.** The bang time  $t_B$  as a function of  $R(t_1, r)$  (curve 0) and of  $R(t_2, r)$  (curve 1) for the model discussed in Section 9.

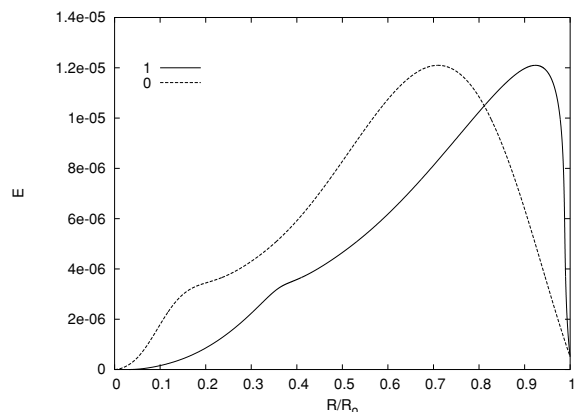


**Figure 15.** The energy function  $E$  as a function of  $R(t_1, r)$  (curve 0) and of  $R(t_2, r)$  (curve 1) for the model discussed in Section 9.

## 10 LIMITATIONS ON THE INITIAL CONDITIONS

An exact reconstruction of the initial conditions that held at the time of decoupling in the region that would become a void is not

possible due to the lack of precise data. Nowadays, the only way to reconstruct the initial conditions is the theoretical approach. The linear theory is often used for this purpose because of its simplicity.

### 10.1 Initial conditions in the linear theory

In linear theory, the shape of the density perturbation is constant in time. Only the amplitude is changing, according to the formula

$$\delta(t) = D\delta_0, \quad (41)$$

where  $\delta_0$  is the current value and  $D$  is the linear growth factor. In the Einstein-de Sitter universe, it is equal to

$$D = \frac{1}{1+z}, \quad (42)$$

and, in the general case,

$$D(a) = \frac{5\Omega_M}{2af(a)} \int_0^a f^3(a') da', \quad (43)$$

where

$$f(a) = \frac{1}{\sqrt{1 + \Omega_M \left(\frac{1}{a} - 1\right) + \Omega_\Lambda (a^2 - 1)}}, \quad (44)$$

while  $a = 1/(1+z)$ . For large redshifts in any model,

$$D(a) \rightarrow \frac{1}{1+z}. \quad (45)$$

In the linear regime in the spherically symmetric case, the peculiar velocity of the density perturbation is given by the formula (Peebles 1993, pp. 115–116)

$$v(r) = -\frac{1}{3}fHSr\delta, \quad (46)$$

where  $H$  is the Hubble constant,  $S$  is the scale factor and  $f$  is the velocity factor. For large redshifts in any cosmological model, this asymptotically becomes unity. Because

$$H = \frac{S_{,t}}{S}, \quad R_{,t} = rS_{,t}, \quad (47)$$

the velocity fluctuations are determined by the formula

$$v = -\frac{1}{3}\delta. \quad (48)$$

That implies that to calculate the evolution of the void one needs the initial density and velocity perturbations with the amplitudes

$$\delta \approx 9 \times 10^{-4}, \quad v \approx 3 \times 10^{-4}. \quad (49)$$

These results are more than 10 times smaller than in the L–T model, where the amplitude needed is  $8 \times 10^{-3}$

Because the current evolution is not linear, one cannot use the linear theory to predict the initial conditions in the young Universe. However, the initial conditions could be obtained with the help of the L–T model, because it is an exact solution of the Einstein field equations. There still remains the question about its accuracy, because the L–T universe is a very simple model of a void. One can try to answer this question by a careful look at the restrictions of the L–T model.

### 10.2 Main limitations of the Lemaître–Tolman model

The L–T model is spherically symmetric, so it cannot take rotation into account. The density and velocity distributions can only depend on the radial coordinate. However, astronomical observations show that for voids these conditions are fulfilled with a satisfactory accuracy.

The next limitation is the dust energy-momentum tensor, which means that the pressure of matter and of radiation are neglected. At

the present epoch this is correct, but one can ask about the error at the moment of the last scattering implied by this assumption. For the purpose of estimating that error, a general Friedmann–Lemaître–Robertson–Walker (FLRW) model will be used.

(i) The pressure: the equation of state for the perfect gas is

$$p = \frac{\rho k_B T}{\mu m_H}, \quad (50)$$

where  $k_B$  is the Boltzmann constant and  $m_H$  is the proton mass. Because of lack of data about the nature of dark matter, let us assume that the mean molecule weight  $\mu = 1$ . In FLRW models,  $T = T_0(1+z)$ , where  $T_0$  is the present value of the background temperature. Substituting the numerical values, we obtain that the ratio of the pressure to the density of matter is

$$\frac{p}{\rho c^2} \approx 2.75 \times 10^{-10}. \quad (51)$$

(ii) The radiation energy density: the expression for the density of the radiation energy is

$$\epsilon_{\text{rad}} = aT^4 = aT_o^4(1+z)^4, \quad (52)$$

where  $a = \frac{4\sigma}{c}$  and  $\sigma$  is the Stefan–Boltzmann constant. The density of matter in the FLRW models is

$$\rho = \rho_o(1+z)^3. \quad (53)$$

If we assume that the present value of density is equal to the critical density in the flat FLRW model, then the ratio of the radiation energy density to the matter energy density will be

$$\frac{\epsilon_{\text{rad}}}{\epsilon_{\text{mat}}} = \frac{aT_o^4}{\rho_o c^2}(1+z) \approx 0.054. \quad (54)$$

From the above, one can see that the gas pressure is negligible. Ignoring the radiation, one makes a small error, which at first seems to be of little importance. However, from the above simulations with different background models, it can be seen that if the initial energy density is higher then the final contrast of matter density is deeper. Unfortunately, this leads to a shorter age of the Universe. To obtain the proper age of the Universe, a higher value of the cosmological constant is needed.

Radiation avoids this problem because during the evolution it becomes less and less significant and the age of the Universe does not change so much. Is it possible then that a model of void formation that includes radiation could predict the voids observed today starting from smaller initial perturbations?

### 10.2.1 Radiation

The Einstein field equations for the spherically symmetric perfect fluid distribution can be reduced to the two following equations (Lemaître 1933):

$$\kappa R^2 R_{,r} \rho c^2 = 2M_{,r}, \quad (55)$$

$$\kappa R^2 R_{,t} p = -2M_{,t}, \quad (56)$$

where  $\rho$  is the energy density, while  $p$  is the pressure.  $M$  is defined by the formula

$$2M(r, t) = R(r, t)R_{,t}^2(r, t) - 2E(r)R(r, t) - \frac{1}{3}\Lambda R^3(r, t). \quad (57)$$

As in the case without radiation,  $Mc^2/G$  is equal to the mass inside the shell of radial coordinate  $r$ . In this case, the mass is not constant in time and in the expanding universe it decreases.

From the equations of motion  $T^{\alpha\beta}_{;\beta} = 0$ , we obtain

$$\begin{aligned} p_{,r} &= 0, \\ p_{,\theta} &= 0, \\ p_{,\phi} &= 0, \end{aligned} \quad (58)$$

$$\rho_{,t} + \left( \rho + \frac{p}{c^2} \right) \left( \frac{2R_{,t}}{R} + \frac{R_{,rt}}{R_{,r}} \right) = 0. \quad (59)$$

Equations (58) require that pressure can only be a function of time. If inhomogeneous radiation should be included in the model, the metric form should be changed: the  $g_{00}$  component should be a function of the radial coordinate. This would require finding a new exact solution of the Einstein equations.

However, it is instructive to know what changes are caused by homogeneous radiation. The time dependence is the same as in the Friedmann models:

$$\begin{aligned} \epsilon_{\text{rad}} &= aT^4 = \epsilon_{\text{dec}} \left( \frac{t_{\text{dec}}}{t} \right)^{8/3}, \\ p_{\text{rad}} &= \frac{1}{3}\epsilon_{\text{rad}}. \end{aligned}$$

For the purpose of comparing with the previous results, the background model is the flat Friedmann model with  $\Lambda = 0$ . The initial density and velocity distributions are presented in Tables 4 and 5.

The computer algorithm implemented to do the calculation was similar to the one used in models without radiation. The only difference is that instead of solving one equation (equation 4), the second-order Runge–Kutta method was used to solve simultaneously equations (56) and (57).

Fig. 16 shows the comparison between the models with and without radiation. The final density contrast in the model with radiation is a little lower inside the void, but higher at the edge compared with the model without radiation.

As one can see, homogeneous radiation is not of great importance in the formation of voids. The difference from the model without radiation is not big because, in spite of higher energy density, as one can see from equation (56), the mass of the shell is decreasing. The decrease of the mass implies, via equation (57) with  $\Lambda = 0$ , that the velocity of the shell is also decreasing with time. Consequently the evolution of the structure slows down and the final results do not show significant differences compared to the model without radiation. These results suggest that the error estimated with equation (54) is indeed of little importance and even the model with inhomogeneous radiation should not lead to significant differences in the final results.

## 11 CONCLUSION

The main aim of this paper was to produce a non-linear model of void formation, starting from small initial density and velocity fluctuations that existed at last scattering, and to investigate what factors are necessary to reproduce current observations.

(i) In the numerical experiments that we carried out, the perturbations that were needed to form a realistic present-day void had to have a density amplitude of  $\delta\rho/\rho \approx 5 \times 10^{-3}$  and a velocity amplitude  $\delta V/V \approx 8 \times 10^{-3}$  (in the model with  $\Omega_{\text{mat}} = 0.27$  and  $\Omega_{\Lambda} = 0.73$ ).

(ii) It was found that density perturbations are of lesser significance than velocity perturbations in the process of void formation.

(iii) There was no significant difference between the evolution of the void in the model with and without the cosmological constant. In this latter case, the amplitude of the initial velocity fluctuation needed for this purpose was a little smaller.

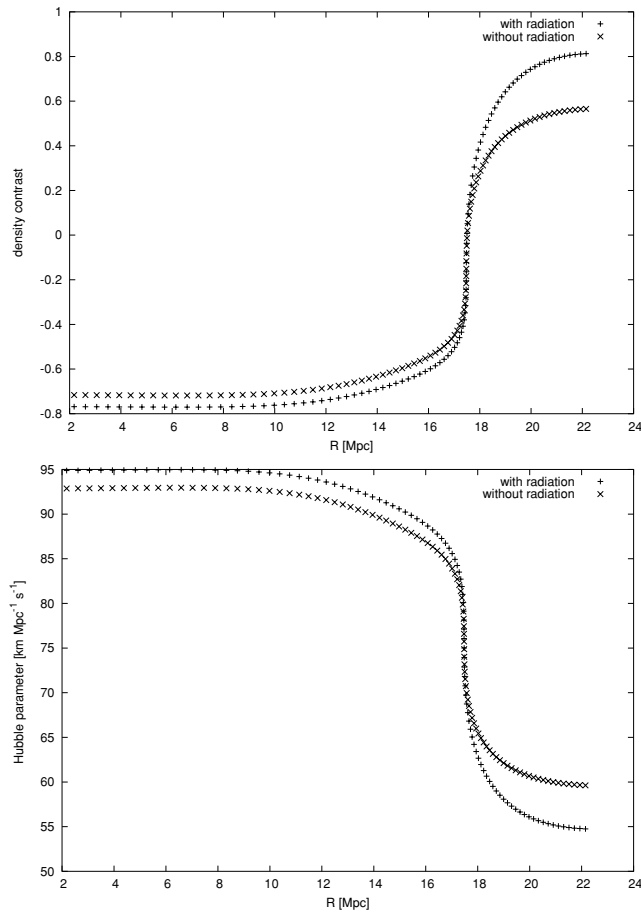


**Figure 16.** The final density contrast and the Hubble parameter in the model with (+) and without (x) the radiation.

(iv) The existence of voids is closely related to the existence of regions of higher density surrounding the voids. In our simulations, there were problems obtaining reasonable profiles for these high-density regions, because shell crossing singularities tended to occur. The L–T model breaks down at shell crossings, so to trace the further evolution of the void we had to focus on the central regions of the void. (In reality, as density increases, a gradient of pressure would appear, which cannot be described in the L–T model.) Because superclusters are observed on the edges of the voids, we interpret this singularity as an indicator of the presence of a supercluster.

Thus, our numerical experiments were not entirely successful at generating a void consistent with observational data, out of perturbations at last scattering that would be as small as indicated by current structure formation theories. Either the initial perturbations had to be larger than the conventional values,  $\delta\rho/\rho \approx 10^{-5} \approx \delta V/c$ , or else the present-day void was too shallow. This discrepancy calls for an explanation. In attempts to explain it, several hypotheses might be considered. We list a set of such hypotheses in the order of decreasing probability of being correct; this is of course our subjective evaluation.

(i) The experiments, here and in Paper II (Kraśniński & Hellaby 2004), showed that the final state is sensitive not just to the amplitude of the initial velocity perturbation, but also to its profile (the density perturbation is less significant). We may not have identified the

profile that gives the best consistency with observations. Work on this will be continued. We tried one approach already, but the results were not encouraging. We took the density distribution in the void at present as given and the density distribution at recombination homogeneous. We calculated the implied velocity distribution at recombination, which was 40 times too large (see Section 8.2.5). Then we numerically decreased the values of that velocity by the factor of 40, took it as part of the input data and calculated the implied density distribution at recombination. It was again too large, so we decreased it numerically by the appropriate factor, took it as input and calculated the implied velocity field at recombination. This iteration quickly converged to stable values of the amplitudes:  $6 \times 10^{-5}$  for density and  $7 \times 10^{-3}$  for velocity. Clearly, this does not solve our main problem.

(ii) Voids may not be as empty as they appear. It is possible they contain a significant amount of unobserved matter, such as gas or other baryonic ‘dark matter’. A present-day density contrast of smaller absolute value is easier to produce with small initial fluctuations.

(iii) Matter may have more components than comoving dust and these other components may be dynamically significant. Including other components in a fully non-linear description and allowing for the possibility that the various kinds of matter do not co-move requires finding solutions of Einstein’s equations with two or more independent streams of matter as a source, which is an extremely challenging problem. Some possible matter components are as follows.

(a) Cold dark matter, i.e. some form of non-baryonic matter that decouples from normal matter very early on and starts forming structures before last scattering. The amplitude of such fluctuations could be larger than what CMB measurements allow for baryonic matter. Whilst there is evidence for some non-luminous matter from galaxy rotation curves, galactic interactions and gravitational lensing, it is less than the required ‘concordance’ value and of unknown composition. The difficulty with this hypothesis is that cold dark matter is not based on any confirmed physical theory and has yet to be detected.

(b) A radiation component that is still significant just after last scattering.

(iv) Observations give the Galaxy distribution in redshift space, and void sizes are deduced by using a Hubble law based on a homogeneous Friedmann model. Because the density distribution thus obtained is clearly not homogeneous, the use of a Friedmann model is really not correct. This may introduce quite significant errors in the density and velocity profiles of voids. The well-known ‘finger of God’ effect is an example of a large discrepancy between true positions and the Friedmann-based mapping from redshift space to physical distances. Consistency with Einstein’s equations requires use of an inhomogeneous cosmological model to correctly map redshift space into physical distances and thus determine how velocities vary with distance. At present, neither the density distribution nor the velocity field of galaxies is known with confidence.<sup>8</sup> Had we known both these fields with a reasonable precision, we might use the L–T model to *calculate* the fluctuations in density and velocity at recombination.

<sup>8</sup> The velocities are measured, but then, without the inconsistent assumption of homogeneity, we do not know to which points in the curved manifold of the Universe they should be attached.

(v) Reliable measurements of temperature fluctuations of the CMB radiation are available only for angular scales larger than  $0^\circ.5$  (see Fig. 2), with the scatter becoming large at  $0^\circ.2$ . On the other hand, as shown in Paper I (Krasiński & Hellaby 2002) and in Section 7.1, the angular diameters, in the CMB sky, of structures the right size to evolve into voids, are less than  $0^\circ.25$ . Though current theory suggests the amplitude decreases at smaller scales, this has yet to be confirmed by improved CMB temperature measurements.

(vi) Solid observational data give the temperature fluctuation of the CMB radiation at present,  $\Delta T/T$ , separately for different modes of perturbation. However, there are several factors contributing to  $\Delta T/T$  (see Section 7.2), which may partially cancel each other. We were interested in the magnitude of the fluid velocity at last scattering, as an initial condition for our models, but we were not able to locate a formula relating the fluid velocity to the observed  $\Delta T/T$ . Thus, our estimate of  $\Delta V$  may be inaccurate. We ourselves do not plan to enter this field, however we would welcome an explicit calculation with a reliable result.

(vii) The Universe may be much older than currently believed, making the time available for void formation much longer. This would require adjustment of the matter content of the universe, of the value of the cosmological constant or of the value of the Hubble constant, each of which may affect the structure-formation time-scale.

(viii) General relativity (GR) may not be the right theory of the evolution of the Universe. There is certainly no lack of proposed modifications or alternatives. While some would gladly accept this conclusion and no-one can claim with certainty that GR will survive all future scrutiny, we wish to stress that GR has a much stronger experimental basis than any cosmic structure formation theory.

## ACKNOWLEDGMENTS

KB wishes to thank the following people who helped him a lot in the work on his MS Thesis, on which this paper is based: his parents for their love and support, his supervisor Andrzej Krasiński for his help with understanding the subject, great patience and heartily smile, Paulina Wojciechowska for all the helpful suggestions and comments, Charles Hellaby, Jacek Jeziński, Fiona Hoyle, Krzysztof Jahn, Michał Chodorowski, Ewa Łokas and Roman Juszkiewicz. CH thanks the South African National Research Foundation for a Core grant and for funding from the Poland—South Africa Technical Cooperation Agreement. AK wishes to thank C. Hellaby and the Department of Mathematics and Applied Mathematics of the Cape Town University, where this paper was finalized, for hospitality and the NRF of South Africa for financing his visit out of the Agreement mentioned above.

## REFERENCES

Arbabi-Bidgoli S., Müller V., 2002, *MNRAS*, 332, 205  
 Bennett C. L. et al., 2003, *ApJS*, 148, 1  
 Benson A. J., Hoyle F., Torres F., Vogeley M. S., 2003, *MNRAS*, 340, 160  
 Bergeron J., Boisse P., 1991, *A&A*, 243, 344

Chincarini G., Rood H. J., 1975, *Nat*, 257, 294  
 Dey A., Strauss M. A., Huchra J., 1990, *AJ*, 99, 463  
 El-Ad H., Piran T., 1997, *ApJ*, 491, 421  
 Gottlöber S., Łokas E. L., Klypin A., Hoffman Y., 2003, *MNRAS*, 344, 715  
 Gregory S. A., Thompson L. A., 1978, *ApJ*, 222, 784  
 Grogin N. A., Geller M. J., 1999, *AJ*, 118, 2561  
 Hoffman G. L., Lu N. Y., Salpeter E. E., 1992, *AJ*, 104, 2086  
 Hoyle F., Vogeley M. S., 2004, *ApJ*, 607, 751  
 Huchra J., Davis M., Latham D., Tonry J., 1983, *ApJS*, 52, 89  
 Jõeveer M., Einasto J., Tago E., 1978, *MNRAS*, 185, 357  
 Kirshner R. P., Oemler A., Schechter P. L., Shectman S. A., 1981, *ApJ*, 248, L57  
 Krasiński A., Hellaby C., 2002, *Phys. Rev. D*, 65, 023501  
 Krasiński A., Hellaby C., 2004, *Phys. Rev. D*, 69, 023502  
 Kuhn B., Hopp U., Elsaesser H., 1997, *A&A*, 318, 405  
 Lanzetta K. M., Bowen D. V., Tytler D., Webb J. K., 1995, *ApJ*, 442, 538  
 Lemaître G., 1933, *Ann. Soc. Sci. Bruxelles*, A53, 51; reprinted in 1997, *Gen. Relativ. Grav.*, 29, 641  
 Lindner U., Einasto J., Einasto M., Freudling W., Fricke K. J., Tago E., 1995, *A&A*, 301, 329  
 Lindner U., Einasto J., Einasto M., Fricke K. J., 1996, preprint (astro-ph/9604108)  
 Mather J. C., Fixsen D. J., Shafer R. A., Mosier C., Wilkinson D. T., 1999, *ApJ*, 512, 511  
 Mayall N. U., 1960, *Ann. Astrophys.*, 23, 344  
 Mustapha N., Hellaby C., 2001, *Gen. Relativ. Grav.*, 33, 455  
 Padmanabhan T., 1996, *Cosmology and Astrophysics Through Problems*. Cambridge Univ. Press, Cambridge  
 Pang T., 1997, *An Introduction to Computational Physics*. Cambridge Univ. Press, Cambridge  
 Peebles P. J. E., 1993, *The Large-Scale Structure of the Universe*. Princeton Univ. Press, Princeton, NJ  
 Peebles P. J. E., 2001, *ApJ*, 557, 495  
 Popescu C. C., Hopp U., Elsaesser H., 1997, *A&A*, 325, 881  
 Press W. H., Flannery B. P., Teukolsky S. A., Vetterling W. T., 1986, *Numerical Recipes*. Cambridge Univ. Press, Cambridge  
 Pustil'nik S. A., Ugryumov A. V., Lipovetsky V. A., Thuan T. X., Guseva N. G., 1995, *ApJ*, 443, 499  
 Rojas R. R., Vogeley M. S., Hoyle F., Brinkmann J., 2004, *ApJ*, 617, 50  
 Rood H. J., 1988, *ARA&A*, 26, 245  
 Sato H., 1982, *Progr. Theor. Phys.*, 68, 236  
 Sato H., 1984, in Bertotti B., de Felice F., Pascolini A., eds, *General Relativity and Gravitation*. D. Reidel and Co., Dordrecht, p. 289  
 Sato H., Maeda K. I., 1983, *Progr. Theor. Phys.*, 70, 119  
 Sen N. R., 1934, *Z. Astrophys.*, 9, 215 (Reprint 1997, *Gen. Relativ. Grav.*, 29, 1477)  
 Spergel D. N. et al., 2003, *ApJS*, 148, 175  
 Steidel C. C., Dickinson M., Persson S. E., 1994, *ApJ*, 427, L75  
 Szomoru A., van Gorkom J. H., Gregg M. D., Strauss M. A., 1996, *AJ*, 111, 2150  
 Thuan T. X., Gott J. R., Schneider S. E., 1987, *ApJ*, 315, L93  
 Tolman R. C., 1934, *Proc. Nat. Acad. Sci. USA*, 20, 169 (Reprint 1997, *Gen. Relativ. Grav.*, 29, 935)  
 Weinberg D. H., Szomoru A., Guhathakurta P., van Gorkom J. H., 1991, *ApJ*, 372, L13  
 Zwaan M. A., Briggs F. H., Sprayberry D., Sorar E., 1997, *ApJ*, 490, 173

This paper has been typeset from a  $\text{\TeX}/\text{\LaTeX}$  file prepared by the author.